

Linear combination estimator of multiple-outcome detections with discrete measurement outcomesL. K. Zhou,^{1,*} J. H. Xu,^{1,*} W.-Z. Zhang,² J. Cheng,² T. S. Yin,¹ Y. B. Yu,¹ R. P. Chen,¹ A. X. Chen,¹
G. R. Jin,^{1,†} and W. Yang^{3,‡}¹Key Laboratory of Optical Field Manipulation of Zhejiang Province and Physics Department of Zhejiang Sci-Tech University,
Hangzhou 310018, China²School of Physical Science and Technology, Ningbo University, Ningbo 315211, China³Beijing Computational Science Research Center, Beijing 100193, China

(Received 3 August 2020; accepted 22 March 2021; published 2 April 2021)

Finding the optimal estimator capable of saturating the Cramér-Rao bound is important for quantum parameter estimation. The maximum likelihood estimator (MLE) is well known to be asymptotically optimal, but it is usually nonanalytic and hence requires extensive numerical computation. On the other hand, the inversion estimator is widely used in experiments due to its simplicity, but it is usually suboptimal. Here we derive an estimator based on the linear combination of multiple inversion estimators associated with the occurrence probability of different measurement outcomes. This linear combination estimator shares the asymptotic optimality of the MLE and the simplicity of the inversion estimator and is applicable to general multi-outcome measurements, irrespective of the specific system and the noise in the system. We demonstrate this estimator for the intensity-difference measurement to a six-photon twin-Fock input state.

DOI: [10.1103/PhysRevA.103.043702](https://doi.org/10.1103/PhysRevA.103.043702)**I. INTRODUCTION**

Quantum-enhancement phase (or parameter) estimation is of importance for multiple areas of scientific research [1–8], including gravitational wave detection [9–11], biological sensing [12,13], atomic clocks [14,15], magnetometry [16], and so on. In experimental works, the phase estimation by inverting the averaged signal is widely used due to its simplicity. According to the central limit theorem, the phase uncertainty of the inversion estimator simply follows error-propagation formula [8]. For instance, the intensity measurement in a Mach-Zehnder interferometer fed by a coherent-state of light exhibits the interferometric signal $\propto \sin^2(\theta/2)$ or $\cos^2(\theta/2)$, which results in the full width at half maximum (FWHM) $=\pi$ and hence the fringe resolution $\Delta x \sim \lambda/2$ (i.e., Rayleigh resolution limit) [17]. Moreover, the achievable phase sensitivity is subject to the standard quantum limit (SQL) $\delta\theta_{\text{SQL}} = 1/\sqrt{\bar{n}}$, where \bar{n} is the number of particles of the input state.

The two classical limits in the sensitivity and in the resolution can be surpassed with nonclassical input states and optimal measurement schemes followed by a proper data processing. In 1981, Caves [9] proposed that the sensitivity can beat the SQL if the two input ports of the interferometer are fed by a coherent state and a squeezed vacuum state of light (i.e., the squeezed-state interferometer). With respect to the squeezed-state interferometer, the photon-counting measurement is optimal to realize the so-called Heisenberg-

limited phase estimation precision [18]. However, this is a non-Gaussian measurement and the achievable sensitivity is subject to the finite number resolution of the photon counters [19,20]. Using a Gaussian measurement (e.g., the homodyne detection at one port of the interferometer [21]), Schäfermeier *et al.* [22] demonstrated the superresolution and the supersensitivity simultaneously, where the measured field quadrature is divided into two bins. A better resolution and an enhanced sensitivity can be realized if one separates the field quadrature into three bins, which can be regarded as a multi-outcome measurement [23].

For a multi-outcome measurement, the inversion estimator is usually suboptimal since it does not take into account all of the available information from the measurement [8]. Therefore, the inversion estimator usually cannot saturate the ultimate phase estimation precision that determined by the Cramér-Rao lower bound (CRB) [1–7]: $\delta\theta_{\text{CRB}} = 1/\sqrt{\mathcal{F}(\theta)}$, where $\mathcal{F}(\theta)$ denotes the classical Fisher information (CFI). Furthermore, some commonly used inversion estimator may not exist in certain cases. For instance, the intensity-difference measurement (i.e., the \hat{J}_z measurement) over the twin-Fock states gives vanishing signal [24,25], which leads to the invalidity of the inversion estimator. To saturate the CRB, the maximum likelihood estimation (MLE) and the Bayesian estimation are usually adopted [26–32]. Particularly, Pezzé *et al.* [26] have demonstrated that the Bayesian estimator can saturate the CRB over a wider phase interval than that of the inversion estimator. Furthermore, the \hat{J}_z measurement followed by the MLE is an optimal protocol for the interferometer fed by the twin-Fock states [30]. This is because the MLE or the Bayesian estimator is unbiased and its uncertainty can saturate the CRB asymptotically. However, the MLE cannot be expressed in an explicit form and its

*These authors contributed equally to this work.

†grjin@zstu.edu.cn

‡wenyang@csrc.ac.cn

evaluation requires much more computational time than that of the inversion estimator. Therefore, it is highly desirable to find an estimator that shares the merits of the MLE (i.e., unbiasedness and asymptotic optimality in the sensitivity) and the inversion estimator (i.e., the simplicity).

Recently, Xu *et al.* [23] proposed a linear combination of multiple inversion estimators and show its application in a three-outcome homodyne detection. However, whether this estimator is valid for other multi-outcome measurements remains unclear. In this work, we present an explicitly analytical form of the composite estimator for a general multi-outcome detection with discrete measurement outcomes. As an example, we consider the \hat{J}_z measurement in the Mach-Zehnder interferometer fed by a six-photon twin-Fock state [33]. Using a Monte Carlo method, we simulate the phase estimation process and show that the composite estimator can saturate the CRB in the asymptotic limit of a large number of repeated measurements. Our result also works for the measurements with continuous-variable outcomes (e.g., the field quadrature) provided that one divides the measurement outcome into several discrete bins, as done by Refs. [21,22]. Therefore, we expect the proposed estimator to find use in various quantum phase-estimation experiments.

II. MULTI-OUTCOME PHASE MEASUREMENTS

For arbitrary multi-outcome measurement, the output signal is the average of an observable $\hat{\Pi} = \sum_k \mu_k \hat{\Pi}_k$ with respect to a phase-encoded state $\hat{\rho}(\theta)$,

$$\langle \hat{\Pi}(\theta) \rangle = \sum_k \mu_k P_k(\theta) \approx \sum_k \mu_k \frac{\mathcal{N}_k}{\mathcal{N}}, \quad (1)$$

where μ_k and $P_k(\theta) = \text{Tr}[\hat{\rho}(\theta)\hat{\Pi}_k]$ denote the eigenvalue and the conditional probability of the k th outcome, with $\{\hat{\Pi}_k\}$ being a discrete set of positive semidefinite measurement operators and satisfying $\sum_k \hat{\Pi}_k = 1$. The probability of each outcome can be measured by the occurrence frequency $\mathcal{N}_k/\mathcal{N}$. For clarity, we refer to \mathcal{N} repeated measurements as a *single run* and use \mathcal{N}_k as the occurrence number of the k th discrete outcome. Obviously, \mathcal{N} is a deterministic integer, but \mathcal{N}_k is a random integer variable, because \mathcal{N}_k may take different values in different runs [averaged at $\mathcal{N}P_k(\theta)$, see the Appendix]. Performing multiple runs at a given $\theta \in (-\pi, \pi)$, one can obtain the phase-dependent probabilities from the statistical average of $\mathcal{N}_k/\mathcal{N}$, which comprises the interferometer calibration [26,33,34]. Next, to estimate an unknown phase shift θ , we perform a single run and obtain a particular set of occurrence numbers $\{\mathcal{N}_k\}$ and construct an unbiased estimator θ_{est} .

Numerically, we adopt a Monte Carlo method to simulate a multi-outcome measurement [18,26,35] using \mathcal{N} random numbers at each θ and recording the occurrence frequencies $\mathcal{N}_k/\mathcal{N}$. After M replicas, the averaged occurrence frequencies are fit as $P_k^{(\text{fit})}(\theta)$. As illustrated by Fig. 1(a), we consider the \hat{J}_z measurement to an N -photon twin-Fock input state $|n, n\rangle_{a,b} \equiv |n\rangle_a \otimes |n\rangle_b$ [24,25], where $N = 2n$ and the subscripts a and b denote two orthogonal modes of the interferometer. The two-mode Mach-Zehnder interferometer can be described by

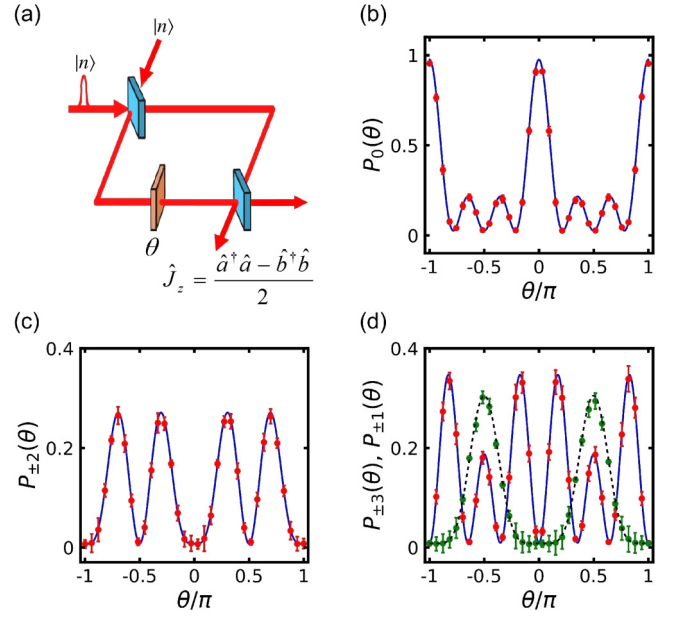


FIG. 1. (a) Light intensity-difference (i.e., \hat{J}_z) measurement at the output ports of the interferometer fed by a N -photon twin-Fock state, and (b)–(d) the occurrence probabilities of $(N + 1)$ -outcome \hat{J}_z measurement with number of photons $N = 6$. The circles and the bars in panels (b)–(d) indicate the mean values of the occurrence frequencies $\mathcal{N}_k/\mathcal{N}$ and their standard deviations, simulated with $M = 20$ replicas of $\mathcal{N} = 500$ random numbers at each a given $\theta \in (-\pi, \pi)$.

a unitary operator (see, e.g., Refs. [8,36])

$$\hat{U}(\theta) = e^{i\frac{\pi}{2}\hat{J}_x} e^{-i\theta\hat{J}_z} e^{-i\frac{\pi}{2}\hat{J}_x} = \exp(-i\theta\hat{J}_y), \quad (2)$$

where $\hat{J} = \frac{1}{2}(\hat{a}^\dagger, \hat{b}^\dagger)\hat{\sigma}(\hat{a}, \hat{b})^T$ denotes Schwinger's representation of the angular momentum, with \hat{a} and \hat{b} being the annihilation operators of the two modes, and $\hat{\sigma} = (\hat{\sigma}_x, \hat{\sigma}_y, \hat{\sigma}_z)$ the Pauli matrix. We adopt eigenstates of \hat{J}_z to express the output state as $|\psi(\theta)\rangle = \hat{U}(\theta)|j, 0\rangle$, where $|j, k\rangle \equiv |j+k, j-k\rangle_{a,b}$ for $k \in [-j, +j]$, with the total spin $j = N/2 = n$. For a N -photon twin Fock state, the \hat{J}_z measurement gives $N + 1$ outcomes, with the occurrence probabilities $P_k(\theta)$. Recently, Xiang *et al.* [33] demonstrated $P_0(\theta)$ as a function of θ for the six-photon twin-Fock state (e.g., $N = 2n = 6$). The probabilities of all the measurement outcomes are shown in Figs. 1(b)–1(d).

Once all phase-dependent $\{P_k(\theta)\}$ and hence the average signal are known, one can infer unknown value of θ via the inversion estimator $\theta_{\text{inv}} = g^{-1}(\sum_k \mu_k \mathcal{N}_k/\mathcal{N})$, where g^{-1} denotes the inverse function of $g(\theta) = \langle \hat{\Pi}(\theta) \rangle$. According to the central limit theorem, the phase uncertainty follows error-propagation formula [8]:

$$\Delta\theta = \frac{1}{\sqrt{\mathcal{N}}} \frac{\Delta\hat{\Pi}}{|\partial\langle\hat{\Pi}\rangle/\partial\theta|}, \quad (3)$$

where $\Delta\hat{\Pi} \equiv (\langle\hat{\Pi}^2\rangle - \langle\hat{\Pi}\rangle^2)^{1/2}$ denotes the root-mean-square fluctuation of the signal. The inversion estimator is widely adopted by experiments due to its simplicity, but it is usually suboptimal. This is because the phase sensitivity per

measurement $\delta\theta \equiv \sqrt{\mathcal{N}}\Delta\theta$ cannot saturate the CRB [1–8]:

$$\delta\theta \geq \delta\theta_{\text{CRB}} \equiv \frac{1}{\sqrt{\mathcal{F}(\theta)}}, \quad (4)$$

where the total CFI and its contribution from each outcome are given by

$$\mathcal{F}(\theta) = \sum_k f_k(\theta), \quad f_k(\theta) = \frac{1}{P_k(\theta)} \left[\frac{\partial P_k(\theta)}{\partial \theta} \right]^2, \quad (5)$$

respectively. It is well known that the MLE saturates the CRB when the number of independent measurements $\mathcal{N} \gg 1$ (see, e.g., Ref. [6]). However, the MLE can only be expressed in a nonanalytic way $\theta_{\text{mle}} = \text{argmax}_\theta \mathcal{P}(\theta|\{\mathcal{N}_k\})$, which is a particular value of θ that maximizes the likelihood function (i.e., a multinomial distribution):

$$\mathcal{P}(\theta|\{\mathcal{N}_k\}) = \mathcal{N}! \prod_{k=1}^m \frac{1}{\mathcal{N}_k!} [P_k(\theta)]^{\mathcal{N}_k}, \quad (6)$$

where m is number of outcomes and $\mathcal{N}_k \equiv \mathcal{N}_k(\theta_0)$ denotes the occurrence number of each outcome at a given true value of phase shift θ_0 . When $\mathcal{N} = \sum_k \mathcal{N}_k \gg 1$, the phase distribution can be well approximated by a Gaussian:

$$\mathcal{P}(\theta|\{\mathcal{N}_k\}) \propto \exp \left[-\frac{(\theta - \theta_{\text{mle}})^2}{2\sigma^2} \right], \quad (7)$$

where σ is a 68.3% confidence interval of the Gaussian around the MLE [18,26,32,37].

A new phase-estimation protocol can be obtained by a convex combination of the CFI of each outcome [23]. Our method starts from the inversion estimator of each outcome $\theta_{\text{inv},k} = P_k^{-1}(\mathcal{N}_k/\mathcal{N})$, which can be obtained by inverting the equation $P_k(\theta) = \mathcal{N}_k/\mathcal{N}$ around θ_0 . Next, we consider the occurrence numbers of each outcome $\mathcal{N}_k \gg 1$ and use Stirling’s formula in Eq. (6):

$$\mathcal{P}(\theta|\{\mathcal{N}_k\}) \approx \frac{1}{\sqrt{(2\pi\mathcal{N})^{m-1}}} \prod_{k=1}^m \frac{1}{\sqrt{P_k(\theta)}} \left[1 + \frac{\xi_k}{P_k(\theta)} \right]^{-(\mathcal{N}_k + \frac{1}{2})}, \quad (8)$$

where we have introduced $\xi_k \equiv \mathcal{N}_k/\mathcal{N} - P_k(\theta) \sim O(\mathcal{N}^{-1/2})$, which are random numbers and satisfy $|\xi_k| \ll P_k(\theta)$ for large enough \mathcal{N} (see the Appendix). To obtain a phase estimator, we further approximate $\mathcal{P}(\theta|\{\mathcal{N}_k\})$ by neglecting the terms up to $O(\mathcal{N}^0)$, and obtain (see the Appendix)

$$\mathcal{P}(\theta|\{\mathcal{N}_k\}) \propto e^{-\mathcal{N}B(\theta)}, \quad (9)$$

where

$$B(\theta) = \sum_{k=1}^m \frac{\xi_k^2}{2P_k(\theta)} = \sum_{k=1}^m \frac{[\mathcal{N}_k/\mathcal{N} - P_k(\theta)]^2}{2P_k(\theta)}. \quad (10)$$

For each outcome, if we consider the single root of the equation $P_k(\theta) = \mathcal{N}_k/\mathcal{N}$ around θ_0 and expand $P_k(\theta)$ as

$$P_k(\theta) \approx P_k(\theta_{\text{inv},k}) + \left. \frac{\partial P_k(\theta)}{\partial \theta} \right|_{\theta_{\text{inv},k}} (\theta - \theta_{\text{inv},k}), \quad (11)$$

then we obtain an approximate result of $B(\theta)$ as

$$\begin{aligned} B(\theta) &\approx \sum_k \frac{1}{2P_k(\theta_{\text{inv},k})} \left(\left. \frac{\partial P_k(\theta)}{\partial \theta} \right|_{\theta_{\text{inv},k}} \right)^2 (\theta - \theta_{\text{inv},k})^2 \\ &= \sum_k \frac{f_k(\theta_{\text{inv},k})}{2} (\theta - \theta_{\text{inv},k})^2, \end{aligned} \quad (12)$$

where we have used the relation $P_k(\theta_{\text{inv},k}) = \mathcal{N}_k/\mathcal{N}$ and $f_k(\theta)$ denotes the CFI associated with the k th outcome, given by Eq. (5). Finally, we obtain the phase estimator using the equation (see the Appendix)

$$\left. \frac{\partial \mathcal{P}(\theta|\{\mathcal{N}_k\})}{\partial \theta} \right|_{\theta_{\text{est}}} \propto \left. \frac{\partial B(\theta)}{\partial \theta} \right|_{\theta_{\text{est}}} = 0, \quad (13)$$

which yields

$$\theta_{\text{est}} = \sum_k c_k \theta_{\text{inv},k}, \quad c_k = \frac{f_k(\theta_{\text{inv},k})}{\sum_{k'} f_{k'}(\theta_{\text{inv},k'})}. \quad (14)$$

The above result has a clear physical meaning as a linear combination of all the inversion estimators $\{\theta_{\text{inv},k}\}$ weighted by the contribution of the Fisher information from each outcome [23]. The performance of θ_{est} can be quantified by M replicas of \mathcal{N} independent measurements at each given θ_0 , which yields the estimators $\{\theta_{\text{est}}^{(1)}, \theta_{\text{est}}^{(2)}, \dots, \theta_{\text{est}}^{(M)}\}$. For large enough \mathcal{N} , the composite estimator is unbiased if $\langle \theta_{\text{est}}^{(i)} \rangle_s - \theta_0$ could be almost vanishing, where $\langle (\dots) \rangle_s \equiv \sum_{i=1}^M (\dots)/M$ denotes the statistical average. Moreover, the composite estimator is optimal if the mean-square error

$$\sigma_{\text{est}} = \sqrt{\langle (\theta_{\text{est}}^{(i)} - \theta_0)^2 \rangle_s} \quad (15)$$

can saturate the CRB $1/\sqrt{\mathcal{N}\mathcal{F}(\theta_0)}$ asymptotically. Before the conclusion of this work, we show that the composite estimator can be regarded as an approximated analytical form of the MLE in the asymptotic limit.

Note that the composite estimator in Eq. (14) is valid for any kind of multi-outcome detection with discrete measurement outcomes, independently from specific system and the noise in the system [38,39]. To obtain θ_{est} , it is important to measure all the probabilities $\{P_k(\theta)\}$ and hence the CFIs $\{f_k(\theta)\}$, as well as the inversion estimators $\theta_{\text{inv},k} = P_k^{-1}(\mathcal{N}_k/\mathcal{N})$. For each k , we need to determine a *unique* solution of $P_k(\theta) = \mathcal{N}_k/\mathcal{N}$, which requires some prior information about θ_0 . When our prior knowledge is sufficient (e.g., there are two solutions $\theta_{\text{inv},k} = 0$ or $\pi/2$, but we already know $\theta_0 \in [-\pi/4, \pi/4]$), this does not cause any problem. However, when our prior knowledge is not sufficient, we cannot determine the inversion estimator uniquely. This problem also occurs not only for the inversion estimator that widely used in experiments (see, e.g., Refs. [26,33,34]), but also for the MLE [40–42]. The standard solution is to use multistep estimation protocol [40–42], or simply a two-step protocol [43].

As the most simplest case, the inversion estimators have been obtained in real experiments by measuring a specific outcome (i.e., a binary-outcome measurement [44,45]). For instance, for the six-photon twin-Fock state [33], it has been shown that the inversion estimator of the outcome $k = 0$ (i.e., measuring equal number of photons at the output ports). For

the N -photon NOON states, the phase uncertainties of $\theta_{\text{inv},0}$ and $\theta_{\text{inv},1/2}$ have been demonstrated for $N = 2$ and 3 [34]. In these two experiments [33,34], the inversion estimator is equivalent to the MLE and therefore its uncertainty follows the CRB (see below). To extract much more phase information, we consider the multi-outcome measurement shown in Fig. 1(a), which can be realized in the experimental setup similar to Ref. [33]. We numerically demonstrate how to obtain the inversion estimators of all the measurement outcomes and therefore the composite estimator.

III. PHASE ESTIMATION WITH THE TWIN-FOCK STATE

As illustrated by Fig. 1(a), we now consider the twin-Fock states as the input of the interferometer. In contrast to a number of entangled states, the twin-Fock states are believed to be robust to the decoherence and hence result in better phase estimation precision under typical experimental noise [27]. However, the \hat{J}_z measurement to the output state $\exp(-i\theta\hat{J}_y)|j, 0\rangle$ gives vanishing signal, due to $\langle\hat{J}_z\rangle = \sum_k k P_k(\theta) = 0$ [25]. This is because the symmetric properties of the occurrence probabilities

$$P_k(\theta) = |\langle j, k | e^{-i\theta\hat{J}_y} | j, 0 \rangle|^2 = [d_{k,0}^j(\theta)]^2, \quad (16)$$

i.e., $P_{-k}(\theta) = P_k(\theta)$ and $P_k(-\theta) = P_k(\theta)$ for $k = -j, -j+1, \dots, +j$. Here $d_{m,n}^j(\theta) = \langle j, m | \exp(-i\theta\hat{J}_y) | j, n \rangle$ denote the Wigner's small d functions, and $j = N/2$ (see, e.g., Ref. [46]). To obtain a phase-sensitive signal, various measurement schemes have been proposed and experimentally demonstrated, such as the parity detection [47–53], the \hat{J}_z^2 measurement [36,54], and the single-fringe detection [33,55]. Particularly, Xiang *et al.* [33] proposed the single-fringe detection to realize high-precision phase measurement beyond the SQL (see below). For the N -photon twin-Fock states, the \hat{J}_z measurement followed by the MLE can achieve a global phase estimation at the Heisenberg limit [30]. However, the ideal result of the CRB, $\delta\theta_{\text{CRB}} = \sqrt{2}/\sqrt{N(N+2)}$, cannot be saturated due to the experimental imperfections.

Inspired by Ref. [33], we numerically simulate the \hat{J}_z measurement over the six-photon twin-Fock state and demonstrate phase-estimation protocol based on Eq. (14). In Figs. 1(b)–1(d), we introduce the experimental imperfections by replacing the occurrence probabilities as

$$P_k^{(\text{im})}(\theta) = A_0 P_k(\theta) + B_k, \quad (17)$$

where $A_0 = 0.9293$, $B_0 = 0.0245$, $B_1 = 0.0087$, $B_2 = 0.0068$, and $B_3 = 0.0076$ (see Ref. [30]). These parameters are chosen such that the symmetric properties of the probabilities remain, i.e., $P_{-k}^{(\text{im})}(\theta) = P_{+k}^{(\text{im})}(\theta)$, which requires $B_{-k} = B_{+k}$. Furthermore, the probabilities satisfy the normalization condition $\sum_k P_k^{(\text{im})}(\theta) = \sum_k P_k(\theta) = 1$. As depicted by Figs. 1(b)–1(d), the occurrence probabilities $P_k^{(\text{im})}(\theta)$ exhibit multifold oscillatory pattern, with the visibility $\approx 92\%$. We show numerical simulations of the occurrence probabilities by using the Monte Carlo method [35], where \mathcal{N} random numbers are generated according to $\{P_k(\theta)\}$ at given $\theta \in (-\pi, \pi)$. Next, we record the occurrence numbers $\{\mathcal{N}_k\}$ and the occurrence frequencies $\{\mathcal{N}_k/\mathcal{N}\}$ of each outcome. Repeating the above processes for M times, we

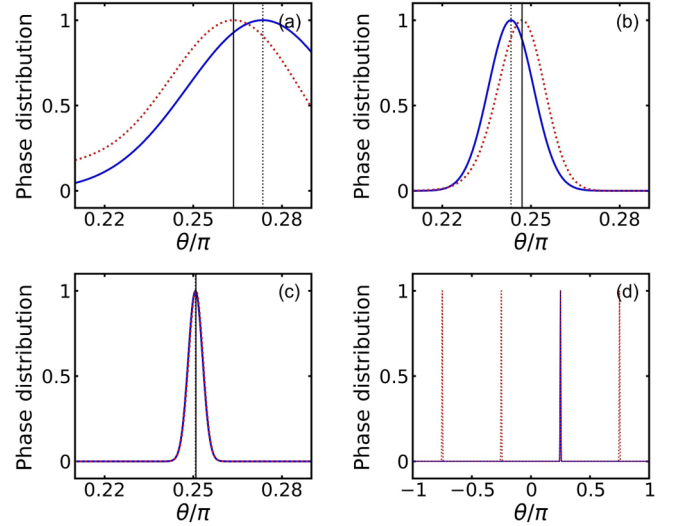


FIG. 2. Phase distribution $\mathcal{P}(\theta|\{\mathcal{N}_k\})$ and its approximate result [i.e., Eqs. (9) and (12)] as a function of θ , simulated with \mathcal{N} random numbers for (a) $\mathcal{N} = 10$, (b) $\mathcal{N} = 100$, (c) $\mathcal{N} = 1000$, (d) full range of panel (c) for $\theta \in (-\pi, \pi)$. The inversion estimators of the \hat{J}_z measurement are obtained by solving the equations $P_k(\theta) = \mathcal{N}_k/\mathcal{N}$, where $k = -j, -j+1, \dots, j$ with $j = N/2 = 3$ and the occurrence numbers \mathcal{N}_k are generated at the true value of the phase shift $\theta_0 = \pi/4$. Red dashed line shows exact result of the phase distribution. Blue solid line shows approximate result of $\mathcal{P}(\theta|\{\mathcal{N}_k\})$.

can obtain the averaged occurrence frequencies (the circles) and their standard deviations (the bars).

Next, we investigate the phase-estimation protocol based upon the composite estimator θ_{est} . In Fig. 2, we compare the exact and the approximate results of $\mathcal{P}(\theta|\{\mathcal{N}_k\})$ to show the validity of θ_{est} , where the approximate result is given by Eq. (9), with $B(\theta)$ given by Eq. (12). Numerically, this can be obtained by generating \mathcal{N} random numbers at θ_0 and recording the occurrence numbers of all the outcomes $\{\mathcal{N}_k\}$. Next, we obtain all the inversion estimators $\{\theta_{\text{inv},k}\}$ by inverting the equations $P_k(\theta) = \mathcal{N}_k/\mathcal{N}$ around θ_0 , where $k = -j, -j+1, \dots, +j$, with $j = N/2 = n$. Then we construct a phase estimator θ_{est} according to Eq. (14). More directly, the estimator θ_{est} is given by the peak of the approximate result, indicated by the vertical dotted lines. One can find that there are significant discrepancies between the exact and the approximate phase distributions for \mathcal{N} up to 100. This is because our protocol requires the conditions $\mathcal{N}_k \sim \mathcal{O}(\mathcal{N})$ and $\mathcal{N} = \sum_k \mathcal{N}_k \gg 1$. As \mathcal{N} increases up to 1000, one can find that the approximate result shows good agreement with the exact result (the red dashed line). Remarkably, the approximate result shows only one peak within a whole phase interval $\theta \in (-\pi, \pi)$. This is because for each outcome we choose the only one root of the equation $P_k(\theta) = \mathcal{N}_k/\mathcal{N}$ near θ_0 . It means that the multipeak structure of $\mathcal{P}(\theta|\{\mathcal{N}_k\})$ [40–42] has been bypassed in solving the inversion estimators $\{\theta_{\text{inv},k}\}$.

In Fig. 3, we show the phase sensitivity $\delta\theta = 1/\sqrt{\mathcal{F}(\theta)}$ for different values of the phase shift, where $\mathcal{F}(\theta)$ is the CFI of the \hat{J}_z measurement and is given by Eq. (5). One can find that the sensitivity can beat the SQL (the upper horizontal

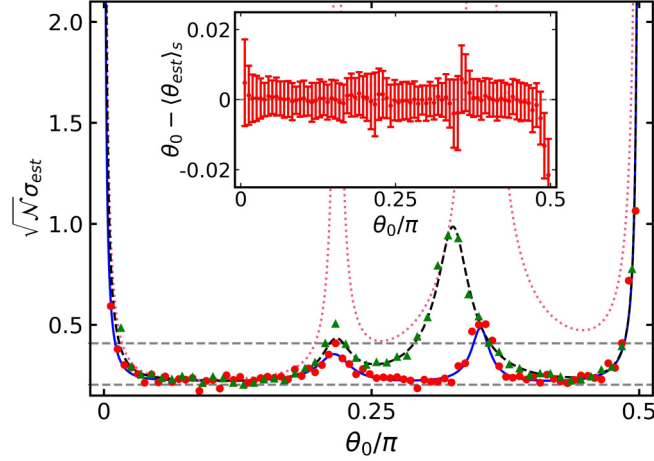


FIG. 3. Phase sensitivities of the \hat{J}_z measurement with and without the coarse-graining against the true value of the phase shift θ_0 , obtained after $M = 200$ replicas of $\mathcal{N} = 2000$ random numbers. The red circles and the blue solid line show the phase uncertainty and the CRB of the \hat{J}_z measurement without the coarse-graining. The triangles and the dashed line show the phase uncertainty and the CRB of the \hat{J}_z measurement with the coarse-graining (i.e., the four-outcome \hat{J}_z measurement). The pink dotted line shows the CRB of the single-fringe measurement $1/\sqrt{\mathcal{F}_2(\theta)}$, where $\mathcal{F}_2(\theta)$ is given by Eq. (18). Horizontal lines: the SQL $1/\sqrt{N}$ and the ideal result of the CRB $\sqrt{2}/\sqrt{N(N+2)}$ for $N = 6$ [30]. Inset shows statistical average of the bias $\theta_0 - \theta_{\text{est}}$ (circles) and its standard deviations (bars), indicating unbiasedness of the composite estimator.

line) over a wide phase interval. Due to the experimental imperfections, the best sensitivity that appeared at the optimal working point $\theta_{\min} \approx 0.11\pi$ (20°) cannot reach the ideal result of the CRB. The circles in Fig. 3 are the phase uncertainties $\sqrt{\mathcal{N}}\sigma_{\text{est}}$, which are obtained by numerical simulation. Specifically, we first obtain all the inversion estimators $\{\theta_{\text{inv},k}\}$ and the composite estimator θ_{est} at each a given value of θ_0 , as shown by Fig. 2. Next, we repeat the above processes for M times to obtain the estimators $\{\theta_{\text{est}}^{(1)}, \theta_{\text{est}}^{(2)}, \dots, \theta_{\text{est}}^{(M)}\}$. Using Eq. (15), one can find that the uncertainty $\sqrt{\mathcal{N}}\sigma_{\text{est}}$ (the circles) almost saturate the CRB (i.e., the blue solid line). The inset in Fig. 3 shows the mean values of θ_{est} (the circles) and their standard deviations (the bars), indicating the unbiasedness of the estimator.

IV. THE PHASE ESTIMATION WITH A COARSE-GRAINING METHOD

In real experiments, it could be difficult to detect all the outcomes of the \hat{J}_z measurement, especially when the number of particles $N \gg 1$ [56–58]. To remedy it, one can adopt a proper coarse-graining method by combining several outcomes into a single one. For instance, as proposed originally by Sun *et al.* [55], Xiang *et al.* have recently demonstrated such a of measurement scheme [33], where they regard $k = 0$ as an outcome (i.e., detecting equal number of photons at the output ports) and all the others detection events as a single one outcome, denoted by $k = \emptyset$. This is the so-called single-fringe detection [33], or equivalently a binary-outcome measurement

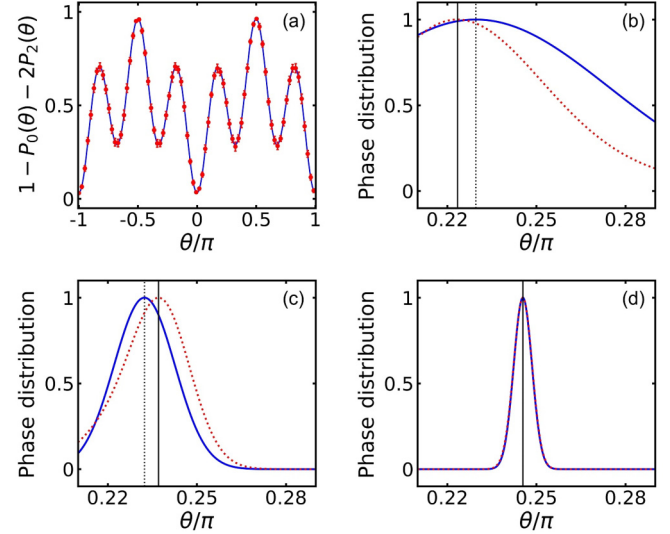


FIG. 4. (a) The occurrence probability of the \hat{J}_z measurement with the coarse-graining method and the phase distributions for different number of the measurements with (b) $\mathcal{N} = 10$, (c) 100, (d) 1000. The solid line in panel (a) is the occurrence probability of the outcome “ \emptyset ” given by $P_\emptyset(\theta) = 1 - P_0(\theta) - 2P_2(\theta)$ with Eq. (17). The circles and the bars in panel (a) are the mean values of the occurrence frequencies $\mathcal{N}_\emptyset/\mathcal{N}$ and their standard deviations, with M and \mathcal{N} the same as in Fig. 1. In panels (b)–(d), the red dotted (blue solid) lines are the exact (approximated) results of $\mathcal{P}(\theta|\{\mathcal{N}_k\})$, where the inversion estimator of each outcome is obtained by inverting the equation $P_k(\theta) = \mathcal{N}_k/\mathcal{N}$ around $\theta_0 = \pi/4$. The vertical lines indicate locations of the composite estimator and the MLE.

[44,45]. The CFI is also given by Eq. (5), namely,

$$\mathcal{F}_2(\theta) = \frac{[P'_0(\theta)]^2}{P_0(\theta)} + \frac{[P'_\emptyset(\theta)]^2}{P_\emptyset(\theta)} = \frac{[P'_0(\theta)]^2}{P_0(\theta)P_\emptyset(\theta)}, \quad (18)$$

where $P'_k(\theta) \equiv \partial P_k(\theta)/\partial \theta$ and $P_\emptyset(\theta) = 1 - P_0(\theta)$. Taking the experimental imperfections into account, i.e., $\{P_k^{(\text{im})}(\theta)\}$, one can obtain the CFI and hence the CRB $\delta\theta = 1/\sqrt{\mathcal{F}_2(\theta)}$; See the dotted line of Fig. 3 (and also Ref. [33]). The sensitivity diverges at the dark points of $P_0^{(\text{im})}(\theta)$, e.g., $\theta_{\text{dark}} = \arctan(\sqrt{2/3}) \approx 0.22\pi$.

To avoid the divergence, one can consider additional contributions of the outcomes $k \neq 0$. For instance, let us consider the outcomes $k = 0$ and ± 2 into the CFI

$$\mathcal{F}_4(\theta) = \frac{[P'_0(\theta)]^2}{P_0(\theta)} + 2\frac{[P'_2(\theta)]^2}{P_2(\theta)} + \frac{[P'_\emptyset(\theta)]^2}{P_\emptyset(\theta)}, \quad (19)$$

where the factor two arises from the symmetry $P_{-2}(\theta) = P_2(\theta)$. Obviously, this is indeed a four-outcome measurement and all the other outcomes $k = \pm 1, \pm 3$ have been treated as a single outcome “ \emptyset ” with the occurrence probability $P_\emptyset(\theta) = 1 - P_0(\theta) - 2P_2(\theta)$ shown in Fig. 4(a). The occurrence probabilities $P_0(\theta)$, $P_2(\theta)$, and thereby $P_\emptyset(\theta)$, can be obtained from the interferometer calibration, as depicted by Figs. 1(b)–1(d).

In Figs. 4(b)–4(d), we show the validity of θ_{est} for the \hat{J}_z measurement with the above coarse-graining method. Similar to Fig. 2, one can find that the approximate result of $\mathcal{P}(\theta|\{\mathcal{N}_k\})$ shows good agreement with that of the exact result

as \mathcal{N} increases up to 1000. For a given $\theta_0 = \pi/4$, the inversion estimator of each outcome is given by $\theta_{\text{inv},k} = P_k^{-1}(\mathcal{N}_k/\mathcal{N})$ with $k = 0, \pm 2, \emptyset$. The peak of $\mathcal{P}(\theta|\{\mathcal{N}_k\})$ gives the location of θ_{est} , which is slightly less accurate in a comparison with that of Fig. 2(c). Theoretically, this is because the coarse-graining method reduces available information about θ_0 and the CRB $\delta\theta = 1/\sqrt{\mathcal{F}_4(\theta)} \geq 1/\sqrt{\mathcal{F}(\theta)}$, where $\mathcal{F}(\theta)$ is the CFI of the \hat{J}_z measurement without the coarse graining.

The performances of θ_{est} with and without the coarse-graining method have been shown in Fig. 3. One can note that the error per measurement (the triangles) almost follow the CRB (the dashed line), i.e., $\sqrt{\mathcal{N}}\sigma_{\text{est}} \approx 1/\sqrt{\mathcal{F}_4(\theta)}$. This means that the protocol based on the composite estimator still works for the coarse-graining method. In addition, one can see that the best sensitivity also appears at the optimal working point $\theta_{\text{min}} \approx 0.11\pi$, similar with that of the \hat{J}_z measurement. When $\theta_0 > \theta_{\text{dark}}$, the achievable sensitivity becomes worse, due to the loss of phase information. However, the sensitivity does not show the divergence at θ_{dark} , better than that of the single-fringe detection [33].

Finally, it should be mentioned that the reason why the composite estimator almost saturates the CRB has not been addressed in Ref. [23]. With a large amount of numerical simulations, especially that of Figs. 2 and 4, we realize that both the exact result of $\mathcal{P}(\theta|\{\mathcal{N}_k\})$ and its approximate one tend to be a Gaussian as $\mathcal{N} \gg 1$. This numerical observation inspires us to rewrite Eq. (9) as Eq. (7), namely,

$$\begin{aligned} \mathcal{P}(\theta|\{\mathcal{N}_k\}) &\propto \exp\left[-\mathcal{N} \sum_k \frac{f_k(\theta_{\text{inv},k})}{2} (\theta^2 - 2\theta_{\text{inv},k}\theta + \theta_{\text{inv},k}^2)\right] \\ &= \exp\left[-\frac{1}{2\sigma_{\text{est}}^2} \left(\theta^2 - 2\theta_{\text{est}}\theta + \frac{\sum_k f_k(\theta_{\text{inv},k})\theta_{\text{inv},k}^2}{\sum_k f_k(\theta_{\text{inv},k})}\right)\right] \\ &\propto \exp\left[-\frac{1}{2\sigma_{\text{est}}^2} (\theta - \theta_{\text{est}})^2\right], \end{aligned} \quad (20)$$

where we have used the approximate result of $B(\theta)$ and introduced $\sigma_{\text{est}} = 1/\sqrt{\mathcal{N} \sum_k f_k(\theta_{\text{inv},k})}$. One can find that the new result of σ_{est} is indeed 68.3% confidence interval of the Gaussian around θ_{est} . Therefore, as an approximated result of the MLE, the composite estimator can saturate the CRB $1/\sqrt{\mathcal{N}\mathcal{F}(\theta_0)}$ asymptotically.

V. CONCLUSION

In summary, we have proposed a phase-estimation protocol based on a combination of the inversion estimators associated with each measurement outcome. As an approximated analytical form of the maximum-likelihood estimator, we show that the composite estimator is valid for arbitrary multi-outcome measurement with discrete outcomes, independently from any specific system and any kind of noise in the system. Numerically, we simulate a $(N+1)$ outcome \hat{J}_z measurement in the interferometer fed by a N -photon twin-Fock state, with $N = 6$ [33]. Our numerical results show that the composite estimator of the system is unbiased and the phase uncertainties saturate the CRB asymptotically. For an N -particle twin-Fock state with $N \gg 1$ [56–58], it may be hard to detect all the outcomes. However, a proper choice of coarse-graining method by combining several outcomes into a single one is possible

to realize the best sensitivity beyond the SQL. We apply this idea to the six-photon twin-Fock state and demonstrate that the composite estimator still works to saturate the CRB.

ACKNOWLEDGMENTS

This project was supported by the Science Foundation of Zhejiang Sci-Tech University (18062145-Y), the National Natural Science Foundation of China (NSFC) (12075209, 12074206, 11704205, 11775190, 11774021, 11874323, 61975184), the Zhejiang Provincial Natural Science Foundation (LZ20A040002), the Open Foundation of Key Laboratory of Optical Field Manipulation of Zhejiang Province (ZJOFM-2019-002), the National Key R&D Program of China (2017YFA0303400), and the NSFC program for ‘‘Scientific Research Center’’ (U1930402).

APPENDIX: DETAILS OF EQ. (9)

When $\mathcal{N}_k \gg 1$, we use the Stirling’s formula $\mathcal{N}_k! \approx \sqrt{2\pi\mathcal{N}_k}(\mathcal{N}_k/e)^{\mathcal{N}_k}$ in Eq. (6), which yields

$$\begin{aligned} \mathcal{P}(\theta|\{\mathcal{N}_k\}) &\approx \sqrt{2\pi\mathcal{N}} \left(\frac{\mathcal{N}}{e}\right)^{\mathcal{N}} \prod_{k=1}^m \frac{(P_k)^{\mathcal{N}_k}}{\sqrt{2\pi\mathcal{N}_k}(\mathcal{N}_k/e)^{\mathcal{N}_k}} \\ &= \frac{1}{\sqrt{(2\pi\mathcal{N})^{m-1}}} \prod_{k=1}^m \left(\frac{\mathcal{N}}{\mathcal{N}_k}\right)^{\mathcal{N}_k + \frac{1}{2}} (P_k)^{\mathcal{N}_k} \\ &= \frac{1}{\sqrt{(2\pi\mathcal{N})^{m-1}}} \prod_{k=1}^m \frac{1}{\sqrt{P_k}} \left(\frac{\mathcal{N}_k}{\mathcal{N}P_k}\right)^{-(\mathcal{N}_k + \frac{1}{2})}, \end{aligned} \quad (A1)$$

where $P_k = P_k(\theta)$. Note that the occurrence numbers $\{\mathcal{N}_k\}$ can be obtained from \mathcal{N} independent measurements (we refer to it as a single run), which are random numbers after multiple runs. For instance, performing M runs, we obtain $\{\mathcal{N}_k^{(1)}, \mathcal{N}_k^{(2)}, \dots, \mathcal{N}_k^{(M)}\}$ for the k th outcome. When M is sufficiently large, the mean value of \mathcal{N}_k and its standard deviation approach $\mathcal{N}P_k$ and $\sqrt{\mathcal{N}P_k(1-P_k)}$, respectively. To further simplify Eq. (A1), we introduce small variables

$$\xi_k = \frac{\mathcal{N}_k}{\mathcal{N}} - P_k, \quad (A2)$$

which gives \mathcal{N}_k and therefore Eq. (8) in the main text. Obviously, ξ_k are also random numbers after the multirun measurements. For a fixed P_k at a given θ , the mean value of ξ_k is almost 0 and its standard deviation approaches $\sigma_k = \sqrt{P_k(1-P_k)}/\mathcal{N} \sim O(\mathcal{N}^{-1/2})$. According to the central limit theorem, the distribution of ξ_k approaches the Gaussian distribution $P(\xi_k) \propto \exp[-\xi_k^2/(2\sigma_k^2)]$ for $\mathcal{N} \gg 1$. As a result, the probability for any particular realization of $|\xi_k| \leq \epsilon$ is well approximated by

$$\Pr(|\xi_k| \leq \epsilon) \approx \text{Erf}\left(\frac{\epsilon}{\sqrt{2}\sigma_k}\right),$$

where $\text{Erf}(\eta)$ is the error function, which rises rapidly to 1 with the increase of η . If we set $\eta = \epsilon/(\sqrt{2}\sigma_k)$, then all realization for $|\xi_k| \leq \epsilon = \sqrt{2}\eta\sigma_k$ occurs with a probability $\text{Erf}(\eta) (\approx 99.99\%$ for $\eta = 2.75)$, which in turn indicates $\xi_k \sim O(\mathcal{N}^{-1/2})$. One can find that all realizations of ξ_k almost lie within a few standard deviations from its mean value 0. On the

other hand, we have $P_k \sim O(\mathcal{N}^0)$ and hence $|\xi_k| \ll P_k$ in the limit of $\mathcal{N} \gg 1$. Note that the result $|\xi_k| \ll P_k$ is also valid even for a very small value of P_k , provided $\mathcal{N} \gg 2\eta^2(1 - P_k)/P_k$. This result can be also obtained by using Hoeffding's inequality.

The approximate result Eq. (8) can be further simplified by using the series expansion $(1+x)^n = \exp[n \ln(1+x)] \approx \exp[nx(1-x/2)]$, namely,

$$\begin{aligned} & \left(1 + \frac{\xi_k}{P_k}\right)^{-(\mathcal{N}_k + \frac{1}{2})} \\ & \approx \exp\left[-\left(\mathcal{N}_k + \frac{1}{2}\right) \frac{\xi_k}{P_k} \left(1 - \frac{\xi_k}{2P_k}\right)\right] \\ & = \exp\left[-\left(\mathcal{N}(\xi_k + P_k) + \frac{1}{2}\right) \frac{\xi_k}{P_k} \left(1 - \frac{\xi_k}{2P_k}\right)\right] \\ & = \exp\left[-\mathcal{N} \frac{\xi_k^2}{2P_k}\right] e^{-\mathcal{N}[\xi_k + O(\mathcal{N}^{-3/2})]}, \end{aligned}$$

which holds for large enough \mathcal{N} and hence $|\xi_k| \ll P_k$, as mentioned above. Therefore, we obtain

$$\begin{aligned} \mathcal{P}(\theta|\{\mathcal{N}_k\}) & \approx \frac{1}{\sqrt{(2\pi\mathcal{N})^{m-1}}} \frac{1}{\sqrt{P_1(\theta)P_2(\theta)\cdots P_m(\theta)}} \\ & \times \exp\left[-\mathcal{N} \sum_{k=1}^m \frac{\xi_k^2}{2P_k(\theta)}\right] e^{-\mathcal{N}[\sum_k \xi_k + O(\mathcal{N}^{-3/2})]} \\ & = A(\theta)e^{-\mathcal{N}B(\theta)} \left[1 + O\left(\frac{1}{\sqrt{\mathcal{N}}}\right)\right], \end{aligned} \quad (\text{A3})$$

where, in the last step, we have used the relation $\sum_k \xi_k = 0$, and introduced the coefficients

$$A(\theta) = \frac{1}{\sqrt{(2\pi\mathcal{N})^{m-1}}} \frac{1}{\sqrt{\prod_{k=1}^m P_k(\theta)}}, \quad B(\theta) = \sum_{k=1}^m \frac{\xi_k^2}{2P_k(\theta)},$$

as Eq. (10) in main text. Obviously, Eq. (A3) can be rewritten as $\mathcal{P}(\theta|\{\mathcal{N}_k\}) \approx A(\theta) \exp[-\mathcal{N}B(\theta)]$ for large \mathcal{N} . Similar to the MLE, the phase estimator θ_{est} is determined by the equation

$$\begin{aligned} 0 & = \left. \frac{\partial \mathcal{P}(\theta|\{\mathcal{N}_k\})}{\partial \theta} \right|_{\theta_{\text{est}}} = \mathcal{P}(\theta|\{\mathcal{N}_k\}) \left[\frac{A'(\theta)}{A(\theta)} - \mathcal{N}B'(\theta) \right] \Big|_{\theta_{\text{est}}} \\ & \propto \left. \frac{\partial B(\theta)}{\partial \theta} \right|_{\theta_{\text{est}}}, \end{aligned} \quad (\text{A4})$$

where the prime indicates the first-order derivation, e.g., $B'(\theta) = \partial B(\theta)/\partial \theta$. The last result of the above equation, i.e., Eq. (13) in main text, comes from the fact that $A'(\theta)/A(\theta)$ is smaller than $\mathcal{N}B'(\theta)$ as $\mathcal{N} \gg 1$, namely,

$$\frac{A'(\theta)}{A(\theta)} = -\frac{1}{2} \sum_{k=1}^m \frac{P'_k}{P_k} \sim O(\mathcal{N}^0), \quad (\text{A5})$$

and

$$\begin{aligned} \mathcal{N}B'(\theta) & = \mathcal{N} \sum_{k=1}^m \frac{-2\xi_k P'_k P_k - \xi_k^2 P'_k}{2P_k^2} \\ & = -\mathcal{N} \sum_{k=1}^m \frac{P'_k \xi_k}{2P_k^2} (2P_k + \xi_k) \\ & \approx -\mathcal{N} \sum_{k=1}^m \frac{P'_k}{P_k} \xi_k \sim O(\mathcal{N}^{1/2}), \end{aligned} \quad (\text{A6})$$

where we have used the relation $\xi'_k = -P'_k$ in the first step and $|\xi_k| \ll P_k$ in the last step. The above results indicate that the role of $A(\theta)$ is negligible. Furthermore, $A(\theta)$ is a slowly varying function in a comparison with $\exp[-\mathcal{N}B(\theta)]$, so we obtain Eq. (9) in main text.

-
- [1] V. Giovannetti, S. Lloyd, and L. Maccone, Quantum-enhanced measurements: Beating the standard quantum limit, *Science* **306**, 1330 (2004).
- [2] V. Giovannetti, S. Lloyd, and L. Maccone, Advances in quantum metrology, *Nat. Photonics* **5**, 222 (2011).
- [3] S. L. Braunstein and C. M. Caves, Statistical Distance and the Geometry of Quantum States, *Phys. Rev. Lett.* **72**, 3439 (1994).
- [4] S. L. Braunstein, C. M. Caves, and G. J. Milburn, Generalized uncertainty relations: Theory, examples, and Lorentz invariance, *Ann. Phys. (NY)* **247**, 135 (1996).
- [5] M. G. A. Paris, Quantum estimation for quantum technology, *Int. J. Quantum Inform.* **7**, 125 (2009).
- [6] C. W. Helstrom, *Quantum Detection and Estimation Theory* (Academic, New York, 1976).
- [7] A. S. Holevo, *Probabilistic and Statistical Aspects of Quantum Theory* (North-Holland, Amsterdam, 1982).
- [8] B. Yurke, S. L. McCall, and J. R. Klauder, Su(2) and su(1, 1) interferometers, *Phys. Rev. A* **33**, 4033 (1986).
- [9] C. M. Caves, Quantum-mechanical noise in an interferometer, *Phys. Rev. D* **23**, 1693 (1981).
- [10] The LIGO Scientific Collaboration, A gravitational wave observatory operating beyond the quantum shot-noise limit, *Nat. Phys.* **7**, 962 (2011).
- [11] J. Aasi *et al.* (The LIGO Scientific Collaboration), Enhanced sensitivity of the LIGO gravitational wave detector by using squeezed states of light, *Nat. Photonics* **7**, 613 (2013).
- [12] M. A. Taylor and W. P. Bowen, Quantum metrology and its application in biology, *Phys. Rep.* **615**, 1 (2016).
- [13] N. Mauranyapin, L. Madsen, M. Taylor, M. Waleed, and W. Bowen, Evanescent single-molecule biosensing with quantum-limited precision, *Nat. Photonics* **11**, 477 (2017).
- [14] A. D. Ludlow, M. M. Boyd, J. Ye, E. Peik, and P. O. Schmidt, Optical atomic clocks, *Rev. Mod. Phys.* **87**, 637 (2015).
- [15] H. Katori, Optical lattice clocks and quantum metrology, *Nat. Photonics* **5**, 203 (2011).
- [16] J. A. Jones, S. D. Karlen, J. Fitzsimons, A. Ardavan, S. C. Benjamin, G. A. D. Briggs, and J. J. L. Morton, Magnetic field sensing beyond the standard quantum limit using 10-spin noon states, *Science* **324**, 1166 (2009).
- [17] A. N. Boto, P. Kok, D. S. Abrams, S. L. Braunstein, C. P. Williams, and J. P. Dowling, Quantum Interferometric Optical Lithography: Exploiting Entanglement to Beat the Diffraction Limit, *Phys. Rev. Lett.* **85**, 2733 (2000).
- [18] L. Pezzé and A. Smerzi, Mach-Zehnder Interferometry at the Heisenberg Limit with Coherent and Squeezed-Vacuum Light, *Phys. Rev. Lett.* **100**, 073601 (2008).

- [19] P. Liu, P. Wang, W. Yang, G. R. Jin, and C. P. Sun, Fisher information of a squeezed-state interferometer with a finite photon-number resolution, *Phys. Rev. A* **95**, 023824 (2017).
- [20] P. Liu and G. R. Jin, Ultimate phase estimation in a squeezed-state interferometer using photon counters with a finite number resolution, *J. Phys. A: Math. Theor.* **50**, 405303 (2017).
- [21] E. Distante, M. Ježek, and U. L. Andersen, Deterministic Super-resolution with Coherent States at the Shot Noise Limit, *Phys. Rev. Lett.* **111**, 033603 (2013).
- [22] C. Schäfermeier, M. Ježek, L. S. Madsen, T. Gehring, and U. L. Andersen, Deterministic phase measurements exhibiting super-sensitivity and super-resolution, *Optica* **5**, 60 (2018).
- [23] J. H. Xu, A. X. Chen, W. Yang, and G. R. Jin, Data processing over single-port homodyne detection to realize superresolution and supersensitivity, *Phys. Rev. A* **100**, 063839 (2019).
- [24] M. J. Holland and K. Burnett, Interferometric Detection of Optical Phase Shifts at the Heisenberg Limit, *Phys. Rev. Lett.* **71**, 1355 (1993).
- [25] C. C. Gerry, R. A. Campos, and A. Benmoussa, Comment on Interferometric Detection of Optical Phase Shifts at the Heisenberg Limit, *Phys. Rev. Lett.* **92**, 209301 (2004).
- [26] L. Pezzé, A. Smerzi, G. Khoury, J. F. Hodelin, and D. Bouwmeester, Phase detection at the quantum limit with multiphoton Mach-Zehnder interferometry, *Phys. Rev. Lett.* **99**, 223602 (2007).
- [27] Z. Zhang and L.-M. Duan, Quantum metrology with Dicke squeezed states, *New J. Phys.* **16**, 103037 (2014).
- [28] W. Larson and B. E. A. Saleh, Supersensitive ancilla-based adaptive quantum phase estimation, *Phys. Rev. A* **96**, 042110 (2017).
- [29] H. T. Dinani, D. W. Berry, R. Gonzalez, J. R. Maze, and C. Bonato, Bayesian estimation for quantum sensing in the absence of single-shot detection, *Phys. Rev. B* **99**, 125413 (2019).
- [30] J. H. Xu, J. Z. Wang, A. X. Chen, Y. Li, and G. R. Jin, Optimal phase estimation with photon-number difference measurement using twin-Fock states of light, *Chin. Phys. B* **28**, 120303 (2019).
- [31] X. Xue, B. D'Anjou, T. F. Watson, D. R. Ward, D. E. Savage, M. G. Lagally, M. Friesen, S. N. Coppersmith, M. A. Eriksson, W. A. Coish, and L. M. K. Vandersypen, Repetitive Quantum Nondemolition Measurement and Soft Decoding of a Silicon Spin Qubit, *Phys. Rev. X* **10**, 021006 (2020).
- [32] H. Strobel, W. Muessel, D. Linnemann, T. Zibold, D. B. Hume, L. Pezzé, A. Smerzi, and M. K. Oberthaler, Fisher information and entanglement of non-Gaussian spin states, *Science* **345**, 424 (2014).
- [33] G. Y. Xiang, H. F. Hofmann, and G. J. Pryde, Optimal multiphoton phase sensing with a single interference fringe, *Sci. Rep.* **3**, 2684 (2013).
- [34] Y. Israel, S. Rosen, and Y. Silberberg, Supersensitive Polarization Microscopy Using NOON States of Light, *Phys. Rev. Lett.* **112**, 103604 (2014).
- [35] J. Z. Wang, Z. Q. Yang, A. X. Chen, W. Yang, and G. R. Jin, Multi-outcome homodyne detection in a coherent-state light interferometer, *Opt. Express* **27**, 10343 (2019).
- [36] T. Kim, O. Pfister, M. J. Holland, J. Noh, and J. L. Hall, Influence of decorrelation on Heisenberg-limited interferometry with quantum correlated photons, *Phys. Rev. A* **57**, 4004 (1998).
- [37] G. R. Jin, W. Yang, and C. P. Sun, Quantum-enhanced microscopy with binary-outcome photon counting, *Phys. Rev. A* **95**, 013835 (2017).
- [38] U. Dorner, R. Demkowicz-Dobrzanski, B. J. Smith, J. S. Lundeen, W. Wasilewski, K. Banaszek, and I. A. Walmsley, Optimal Quantum Phase Estimation, *Phys. Rev. Lett.* **102**, 040403 (2009).
- [39] Y. M. Zhang, X. W. Li, W. Yang, and G. R. Jin, Quantum Fisher information of entangled coherent states in the presence of photon loss, *Phys. Rev. A* **88**, 043832 (2013).
- [40] L. Pezzé and A. Smerzi, Sub shot-noise interferometric phase sensitivity with beryllium ions Schrödinger cat states, *Europhys. Lett.* **78**, 30004 (2007).
- [41] B. L. Higgins, D. W. Berry, S. D. Bartlett, H. M. Wiseman, and G. J. Pryde, Entanglement-free Heisenberg-limited phase estimation, *Nature (London)* **450**, 393 (2007).
- [42] D. W. Berry, B. L. Higgins, S. D. Bartlett, M. W. Mitchell, G. J. Pryde, and H. M. Wiseman, How to perform the most accurate possible phase measurements, *Phys. Rev. A* **80**, 052114 (2009).
- [43] M. Hayashi, S. Vinjanampathy, and L. C. Kwak, Resolving unattainable Cramer-Rao bounds for quantum sensors, *J. Phys. B: At., Mol. Opt. Phys.* **52**, 015503 (2019).
- [44] X. M. Feng, G. R. Jin, and W. Yang, Quantum interferometry with binary-outcome measurements in the presence of phase diffusion, *Phys. Rev. A* **90**, 013807 (2014).
- [45] L. Ghirardi, I. Siloi, P. Bordone, F. Troiani, and M. G. A. Paris, Quantum metrology at level anticrossing, *Phys. Rev. A* **97**, 012120 (2018).
- [46] X. M. Feng, P. Wang, W. Yang, and G. R. Jin, High-precision evaluation of Wigner's d matrix by exact diagonalization, *Phys. Rev. E* **92**, 043307 (2015).
- [47] J. J. Bollinger, W. M. Itano, D. J. Wineland, and D. J. Heinzen, Optimal frequency measurements with maximally correlated states, *Phys. Rev. A* **54**, R4649 (1996).
- [48] C. C. Gerry, Heisenberg-limit interferometry with four-wave mixers operating in a nonlinear regime, *Phys. Rev. A* **61**, 043811 (2000).
- [49] C. C. Gerry, A. Benmoussa, and R. A. Campos, Nonlinear interferometer as a resource for maximally entangled photonic states: Application to interferometry, *Phys. Rev. A* **66**, 013804 (2002).
- [50] C. C. Gerry and J. Mimihi, The parity operator in quantum optical metrology, *Contemp. Phys.* **51**, 497 (2010).
- [51] P. M. Anisimov, G. M. Raterman, A. Chiruvelli, W. N. Plick, S. D. Huver, H. Lee, and J. P. Dowling, Quantum Metrology with Two-Mode Squeezed Vacuum: Parity Detection Beats the Heisenberg Limit, *Phys. Rev. Lett.* **104**, 103602 (2010).
- [52] A. Chiruvelli and H. Lee, Parity measurements in quantum optical metrology, *J. Mod. Opt.* **58**, 945 (2011).
- [53] K. P. Seshadreesan, S. Kim, J. P. Dowling, and H. Lee, Phase estimation at the quantum Cramér-Rao bound via parity detection, *Phys. Rev. A* **87**, 043833 (2013).
- [54] B. Lücke, M. Scherer, J. Kruse, L. Pezzé, F. Deuretzbacher, P. Hyllus, O. Topic, J. Peise, W. Ertmer, J. Arlt *et al.*, Twin matter waves for interferometry beyond the classical limit, *Science* **334**, 773 (2011).
- [55] F. W. Sun, B. H. Liu, Y. X. Gong, Y. F. Huang, Z. Y. Ou, and G. C. Guo, Experimental demonstration of phase measurement precision beating standard quantum limit by projection measurement, *Europhys. Lett.* **82**, 24001 (2008).

- [56] Z. Zhang and L.-M. Duan, Generation of Massive Entanglement Through an Adiabatic Quantum Phase Transition in a Spinor Condensate, *Phys. Rev. Lett.* **111**, 180401 (2013).
- [57] X.-Y. Luo, Y.-Q. Zou, L.-N. Wu, Q. Liu, M.-F. Han, M. K. Tey, and L. You, Deterministic entanglement generation from driving through quantum phase transitions, *Science* **355**, 620 (2017).
- [58] Y.-Q. Zou, L.-N. Wu, Q. Liu, X.-Y. Luo, S.-F. Guo, J.-H. Cao, M. K. Tey, and L. You, Beating the classical precision limit with spin-1 Dicke states of more than 10,000 atoms, *Proc. Natl. Acad. Sci. USA* **115**, 6381 (2018).